

RESEARCH ARTICLE

A New Causal Rule Learning Approach to Interpretable Estimation of Heterogeneous Treatment EffectYing Wu^a, Hanzhong Liu^b, Kai Ren^c, Shujie Ma^d and Xiangyu Chang^a

^aDepartment of Information Systems and Intelligent Business, School of Management, Xi'an Jiaotong University, Xi'an, 710049, Shaanxi, P.R.China; ^b Department of Industrial Engineering, Tsinghua University, 100084, Beijing, P.R.China; ^c Department of Cardiovascular Surgery, Xijing Hospital, Air Force Military Medical University, Xi'an, 710032, Shaanxi, P.R.China; ^d Department of Statistics, University of California-Riverside, Riverside, CA 92521, U.S.A.

ARTICLE HISTORY

Compiled February 25, 2025

ABSTRACT

Interpretability plays a critical role in the application of statistical learning for estimating heterogeneous treatment effects (HTE) for complex diseases. In this study, we leverage a rule-based workflow, namely causal rule learning (CRL) to estimate and enhance our understanding of HTE for atrial septal defect, addressing an overlooked question in previous literature: what if an individual simultaneously belongs to multiple groups with different average treatment effects? The CRL process consists of three steps: rule discovery, which generates a set of causal rules with corresponding subgroup average treatment effects; rule selection, which identifies a subset of these rules to deconstruct individual-level treatment effects as a linear combination of subgroup-level effects; and rule analysis, which outlines a detailed procedure for further analyzing each selected rule from multiple perspectives to identify the most promising rules for validation. Extensive simulation studies and real-world data analysis demonstrate that CRL outperforms other methods in providing interpretable estimates of HTE, especially when dealing with complex ground truth and sufficient sample sizes.

KEYWORDS

Heterogeneous treatment effect; interpretability; rule-based method; atrial septal defect; healthcare decision-making

1. Introduction

In clinical research and practice, patients respond differently to certain treatment interventions, necessitating the exploration of heterogeneous treatment effects (HTE) to inform personalized treatment plans and optimize health outcomes. From a practitioner's perspective, this exploration requires not only accurate estimation but also a deep understanding of HTE, which can be challenging to achieve in real clinical treatment [12], especially for complex diseases such as atrial septal defect (ASD). As a common type of congenital heart disease, ASD presents various pathologies and heterogeneity in patients [8]. With accurate HTE estimation and enhanced interpretation of

CONTACT Ying Wu: yingwu@stu.xjtu.edu.cn; Hanzhong Liu: lhz2016@tsinghua.edu.cn; Kai Ren: rk90108@163.com; Shujie Ma: shujie.ma@ucr.edu; Xiangyu Chang: xiangyuchang@xjtu.edu.cn

HTE estimates, cardiologists are able to understand, trust, and justify their treatment recommendations, fostering doctor-patient communication and collaboration [12, 20].

So far, researchers have made great efforts to estimate HTE accurately using various methods, among which statistical learning methods are particularly popular due to their ability to handle high-dimensional datasets and uncover non-linear relationships between covariates [37, 45, 50, 51]. However, most methods are typically designed for general estimation purposes, lacking specific adaptations for clinical applications. Stepping back, they seldom provide guidance on how to interpret what their model has learned from the data. Consequently, clinicians may find it hard to understand these methods, let alone the application of them in real practice.

There has been increasing research to deal with the above interpretability issue in HTE estimation [10, 13, 15, 17, 22, 47], and the majority focuses on identifying subgroups with enhanced (positive) treatment effect. However, the setup and methodology of these studies may be far from sufficient to reveal the complex nature of certain diseases. For complex disease treatment whose outcome is influenced by a lot of factors and interactions among these factors, we may find the situation shown in Figure 1: There are M true subgroups (from subgroup 1 to subgroup M) that contribute to treatment effect heterogeneity. The population within each subgroup (e.g., subgroup 1) shares the same treatment effect ($\tau_1 = 20$), i.e., subgroup conditional average treatment effect (CATE) derived from the difference between two treatment groups within the subgroup. The subgroup CATEs between groups vary in effect size (or magnitude) and sign ($\tau_2 = 15$ and $\tau_3 = -8$). Besides, these subgroups are characterized with (not necessarily) different features, such as subgroup 1 by $chdhis \leq 1$ and $diabp \leq 58$ or subgroup 2 by $NYHA \leq 1$ and $BMI \leq 16.02$. Therefore, when we find the individual belongs to subgroups 1, 2, and M ($r_1 = 1, r_2 = 1, r_M = 1$) at the same time (multiple memberships), it raises the question of what the individual level treatment effect (ITE) should be, given the three subgroups differ in treatment effect. Considering the complex nature of certain diseases, we assume ITE as *a linear combination of the above candidate group CATE* in this study. Hence, the ITE in Figure 1 is $1/3 \times 20 + 1/5 \times 15 + 1/10 \times (-7) = 173/21$ where $\beta_1 = 1/3$, $\beta_2 = 1/5$, and $\beta_M = 1/10$ are the linear coefficients in the combination which quantifies the contribution of each candidate subgroup to ITE.

Compared with our perspective, the studies focus on subgroup identification usually end up with a limited number of subgroups for interpretability concern [11, 44] (e.g., only subgroup 1 and 2 in Figure 1 are identified). Some approaches even define mutually disjoint subgroups (e.g., [47]): One individual can only belong to one subgroup. As indicated in [44], individual effects are not guaranteed to have even the same sign as CATE, not to mention the same magnitude. Therefore, an ITE cannot be determined solely by belonging to a few specific groups, which relates to a few covariates. On the contrary, ITE may involve a broader range of subgroup memberships, and we need to consider how being in these subgroups collectively influences an individual, i.e., to explore the relationship between individual-level treatment effects and group-level treatment effects. In addition, since these studies emphasize a few subgroups, they are likely to ignore the estimation and understanding of ITE for the population outside the identified subgroups.

With consideration of the above, this study introduces a novel method, Causal Rule Learning (CRL), to integrate both accurate estimation and an in-depth understanding of HTE for complex diseases. Guided by the Predictive, Descriptive, Relevant (PDR) framework of interpretability [31] (see Appendix A for more information) and inspired by the RuleFit [16] methodology, CRL caters to healthcare practitioners via an easily

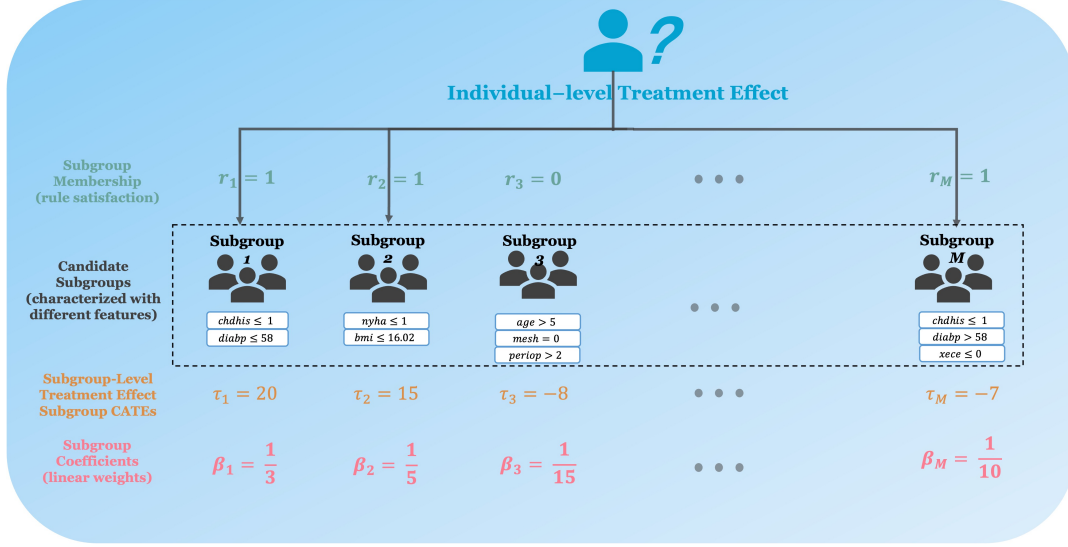


Figure 1. Connection between individual level and subgroup level treatment effects.

understood rule-based approach and an enlightening perspective on the relationship between ITE and CATE. Specifically, CRL incorporates three steps, i.e., rule discovery, rule selection, and rule analysis. The rule discovery step first generates a set of causal rules (characterized by different patient covariates) and their corresponding subgroup CATE estimates using causal forest [45]. Then, the rule selection step leverages a D-learning method [34] to filter out non-informative rules and use the informative ones to estimate ITE. Lastly, the rule analysis step evaluates the rules from three different granularity levels, namely overall analysis, significance analysis, and decomposition analysis. The whole workflow with details is shown in Figure 2.

CRL contributes to the existing literature and healthcare practice by enriching the toolset for interpretable HTE estimation, particularly in scenarios involving complex disease treatments. In detail, we propose:

- (1) A comprehensively interpretable framework for HTE estimation. CRL presents an end-to-end rule-based workflow that includes the discovery, selection, and analysis of rules. Rules are used for their easiness in human understanding, usefulness in healthcare practice, and inclusion of potential knowledge. The discovery step seeks large candidates of rules, which is meaningful for revealing the unknown aspects of HTE. The following selection step imposes sparsity on these rules, surfacing the most predictive and promising ones for ITE and further analysis. The analysis step provides an in-depth investigation of the rules identified, ranging from the overall performance of the rules as a whole on HTE-related tasks to how each component contributes to a specific rule on differentiating effect magnitudes, providing in-depth interpretation of the subgroups identified.
- (2) A novel perspective integrating group and individual-level treatment effects: ITE as a linear combination of subgroup CATE. This perspective attempts to explore and make clear the relationship between ITE and CATE, which answers a previously overlooked yet practically relevant question: What occurs when an individual patient belongs to multiple subgroups with different average treatment effects? By bridging subgroup characteristics with individual-level outcomes, we

can build a deeper and more structured understanding of treatment heterogeneity that may align with the truth of complex diseases.

Together, the refined rules, their corresponding subgroup CATEs, and weights (coefficients in the linear combination) obtained after the whole workflow provide insights to clinicians as clinical hypotheses for future validation through clinical trials and large-scale studies, enabling actionable suggestions in healthcare practice.

The rest of this paper is organized as follows: In Section 2, we briefly summarize previous studies on HTE for clinical purposes. Section 3 delineates the proposed CRL workflow, including its basic data settings and assumptions, formulation, and workflow. Section 4 demonstrates the efficacy of CRL on both simulated data and real-world data, respectively. Section 5 concludes our work and discusses its limitations and potential future research directions. For brevity in this paper, we will slightly misuse the following terms: i) HTE, CATE, and ITE; ii) *satisfy a rule* and *belongs to a subgroup*. These terms are used according to specific contexts and sometimes indiscriminately in broader situations.

2. Related work

This section presents extant literature related to HTE estimation from various perspectives. The majority of studies focus on the estimation of CATE, namely the average treatment effect on specific subgroups. A small strand of research aims at treatment recommendation, i.e., directly modeling the best individualized treatment rules or policy given personal characteristics to maximize the outcome of interest. Weighting methods are frequently used for this goal, such as [19, 29, 50, 51]. Though the latter is capable of providing actionable suggestions to clinical treatment decisions, they often fail to give explicit decision rationale or insights into HTE, which is really crucial for complex disease treatment. Therefore, we mainly discuss the studies on CATE estimation below.

CATE research generally has two focal points. One is developing general CATE estimators with favorable statistical properties using statistical methods such as single-index models [14, 38] or (causal) machine learning methods such as causal forest [5] and meta-learners [18, 32, 42]. Some studies involve complicated computations or even black-box models [1, 26, 48] that are inherently unexplainable to improve estimation accuracy, failing to provide sufficient interpretation catering to clinical practitioners. The other focus emphasizes identifying and characterizing subgroups with statistically significant and practically meaningful heterogeneity in treatment response, such as [9, 39]. Tree-based methods such as [17, 30, 37, 39] have a natural advantage for this end due to their heuristic mechanism on population segmentation.

In particular, there is a growing field of CATE studies with rule ensemble models that follow quite different philosophies and workflows. As examples, [13] proposes a method called Stable Discovery of Interpretable Subgroups via Calibration to discover interpretable and stable rule sets from well-calibrated samples across 18 popular CATE estimators. Similarly, [28] uses multiple CATE estimators as outcomes to generate tree ensembles for rule generation and then prune the rules with certain penalties. They re-estimate CATE for the subpopulation characterized by the remaining rules. [47] proposes Causal Rule Sets to identify subgroups with enhanced treatment effect through a generative Bayesian framework that assumes a prior for the actual rule set and a Bayesian logistic regression model to improve it. As mentioned earlier, all

these studies presume a limited number of true subgroups which may lead the truth of complex disease under-explored, especially for the population outside the identified subgroups.

3. Causal Rule Learning

3.1. Preliminaries

3.1.1. Notation and assumptions

We consider a triplet (X, A, Y) where $X = (x_1, x_2, \dots, x_p)^\top$ denotes a p -dimensional vector of sample characteristics (covariates) and $A \in \mathcal{A} = \{-1, 1\}$ represents the treatment received, with -1 indicating negative treatment (or control) and 1 indicating positive treatment. Correspondingly, we have $Y(1), Y(-1) \in \mathbb{R}$ denote the potential outcomes for the two treatments, and $Y = Y(A)$ is the observed outcome. In this paper, we assume that higher values of Y are preferred.

Suppose that we have observed a data set $\mathcal{D} = \{X_i, A_i, Y_i\}_{i=1}^N$ which comprises N independent and identically distributed samples. This data set may come from an observational study or, more ideally, a randomized controlled trial (RCT) setting. The proposed framework can be applied to data from both settings but requires the satisfaction of the three basic assumptions of the Neyman–Rubin potential outcome framework [35, 36], namely the Stable Unit Treatment Value Assumption, Unconfoundedness Assumption, and Overlap Assumption. Details of these assumptions are given in Appendix B.

3.1.2. Individualized treatment effect based on causal rules (subgroup CATE)

In this study, we estimate ITE directly through a set of causal rules. By causal rules, we mean that the rules are identified from a causal analysis framework. As a natural way to represent human knowledge and a widely-used tool in clinical guidelines, they uncover variables’ potential interaction (synergistic effect) and define certain subgroups to help us understand the heterogeneity of the treatment effect. Most importantly, [16] and [31] show evidence that rule-based models have comparable and sometimes even better performance than black box methods like neural networks. Therefore, rules match our needs for both accuracy and interpretability. This paper formulates a rule as:

$$r(X) = \prod_{j=1}^p 1(x_j \in s_j), \quad (1)$$

where x_j denotes the j -th element of X , s_j is a specified subset of all values of x_j , and $1(\cdot)$ is the indicator function yielding 1 when $x_j \in s_j$ and 0 otherwise. For example, $x_1 > 0$ and $x_2 < 0$ and $x_3 > 5$ is a rule representation consisting of three components. Each component (e.g., $x_1 > 0$) has a splitting variable (x_1) and a given cut-off value or threshold (0), which defines s_1 . A rule $r(X)$ maps an input X into $\{0, 1\}$, representing the satisfaction of a rule with 1 and 0 otherwise. Note that a rule is usually represented only by the variables that help to split the whole population, and the ones that do not are often ignored.

As a formulated version of Figure 1, the ITE can be represented by:

$$\tau(X) := \sum_{m=1}^M \beta_m \tau_m r_m(X), \quad (2)$$

where $r_m(X)$, τ_m , and β_m denote the satisfaction of the m -th rule (0 or 1) given X , its corresponding subgroup CATE and weight in the linear combination respectively. Each subgroup CATE has a different contribution to ITE, as reflected by the sign and magnitude of the weights β and the subgroup CATEs. More significant absolute values of these quantities imply more contribution. Given above, the problem then boils down to the revelation of $\{r_m(X), \tau_m, \beta_m\}_{m=1}^M$. Various methods can be used to find the rules and estimate the quantities. The final choice is up to the particular problem and intended audience. The next section shows our CRL framework to achieve these goals.

3.2. CRL Workflow

3.2.1. Rule discovery via causal forest

Our model utilizes causal forests [45] to derive the initial set of potential rules and corresponding CATE estimates. Causal forest is a non-parametric method for heterogeneous treatment effect estimation whose estimator has been shown to have good statistical properties like point-wise consistency and asymptotical normality for the true CATE under the three Neyman-Rubin assumptions [45].

A causal forest consists of many causal trees [3], each trained using a random subsample of observations and covariates. Given a causal tree, it is easy and intuitive to decompose the tree into multiple rules: the path from the root to a leaf node naturally forms a rule formulated in definition (1). Instances within a leaf node directly make up a potential subpopulation. Further, we use the following plug-in estimator of difference-in-means as an estimate for the corresponding CATE of a given subgroup G in a leaf node:

$$\hat{\tau}_G = \frac{\sum_i Y_i 1(A_i = 1, X_i \in G)}{\sum_i 1(A_i = 1, X_i \in G)} - \frac{\sum_i Y_i 1(A_i = -1, X_i \in G)}{\sum_i 1(A_i = -1, X_i \in G)}. \quad (3)$$

3.2.2. Rule selection with the D-learning method

Due to the randomization and greediness introduced by forest-based methods, fake and redundant rules are inevitably generated [46]. The rule selection process aims to filter out those irrelevant and unnecessary rules from the initial rule set to improve the accuracy of ITE estimation and size down the rule set for interpretability purposes.

For this end, we leverage the D-learning method [34] to learn a sparse combination of rules that can estimate ITE accurately. The original D-learning method aims to directly learn the optimized individual treatment rule (ITR) $d^*(X)$ in a single step without model specification, defined as:

$$d^*(X) = \text{sign}\left(\mathbf{E}\left[\frac{YA}{\pi(A, X)}|X\right]\right) = \text{sign}(\tau^*(X)), \quad (4)$$

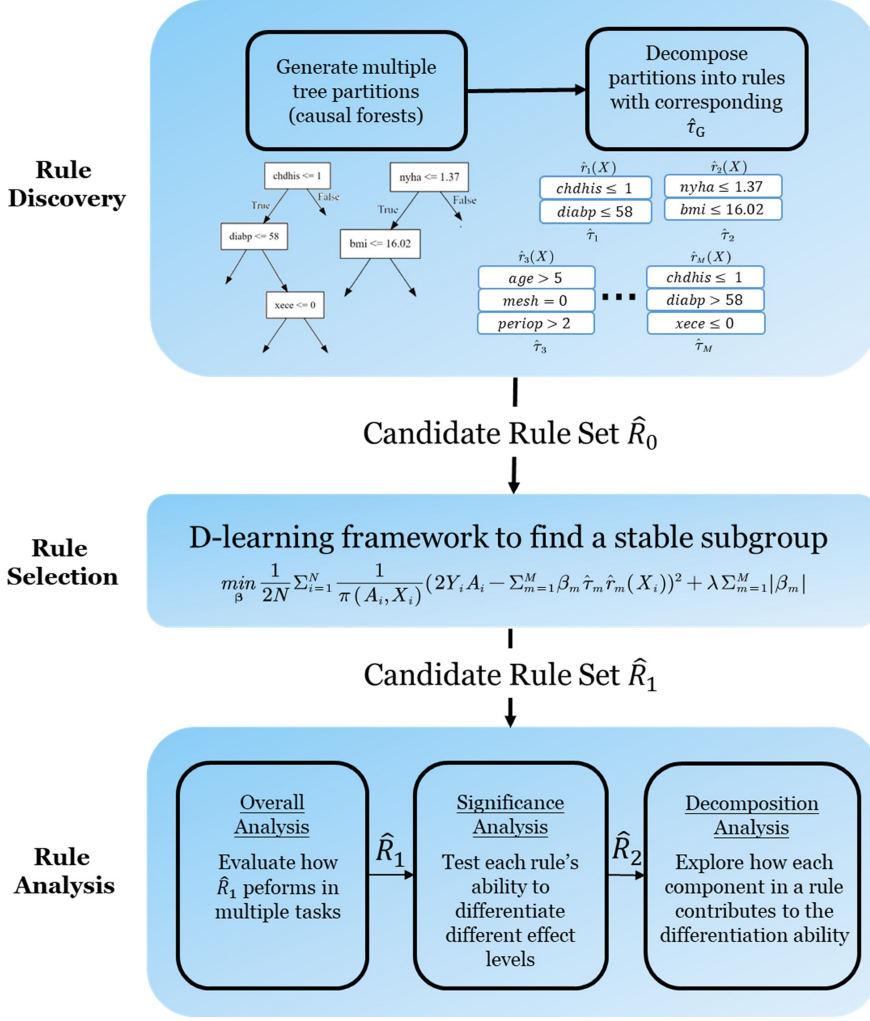


Figure 2. Workflow of causal rule learning.

where the expectation $\mathbf{E}[YA/\pi(A, X)]$ or $\tau^*(X)$ is the exact desired ITE. (4) leverages the propensity score defined as the probability of receiving treatment a given X , i.e., $\pi(A, X) = Pr(A|X)$. For RCT data, we assume this score is already known. For observational data, we have to specify a proper model and learn the score from the data.

It has been proved in [34] that under the assumption of interchange between differentiation and expectation,

$$\tau^*(X) \in \arg \min_{\tau(X)} \mathbf{E} \left[\frac{(2YA - \tau(X))^2}{\pi(A, X)} | X \right],$$

which transforms the estimation of unobserved ITE into an expectation minimization problem where $\tau(X)$ can be any proper form, allowing a flexible specification no matter linear or nonlinear.

Therefore, replacing $\tau(X)$ with a linear combination of subgroup CATE, i.e., the right-hand side of (2) and imposing additional ℓ_1 penalty on the weights of the rules to ensure sparsity, we can reformulate the estimation of $\tau^*(X)$ as a ℓ_1 penalized regres-

sion problem and obtain the least absolute shrinkage and selection operator (LASSO) estimator [41] of the rule weights $\hat{\beta}^{lasso}$:

$$\hat{\beta}^{lasso} = \arg \min_{\beta} \left\{ \frac{1}{2N} \sum_{i=1}^N \frac{1}{\pi(A_i, X_i)} \{2Y_i A_i - \sum_{m=1}^M \beta_m \hat{\tau}_m \hat{r}_m(X_i)\}^2 + \lambda \sum_{m=1}^M |\beta_m| \right\}, \quad (5)$$

where $\lambda > 0$ is the tuning parameter that controls the degree of penalty. Then we can easily obtain CRL estimates of ITE: $\hat{\tau}_{CRL}(X) = \sum_{m=1}^M \hat{\beta}_m^{lasso} \hat{\tau}_m \hat{r}_m(X)$.

Just as [31] states, when we impose sparsity on our model, we limit the number of non-zero parameters in the model and interpret the rules corresponding to those parameters (based on sign and magnitude) as meaningful to the outcome of interest. Since a large number of weights are zero (i.e., $\hat{\beta}^{lasso}$ usually has many elements equal to 0), their corresponding rules are actually removed from the candidate set and make no contribution to our estimator. Imposing this sparsity of rules also highlights the distinction between our CRL estimator and the causal forest estimator, which simply takes the average over all the tree estimates (subgroup CATEs in our method) as the final estimates, while our method learns a weighted combination of those estimates. In other words, we reweight the tree estimates instead of using them equally. In this sense, causal forest estimates can be viewed as a special case of our method. We show in Figure 4(d) that reweighting the rules with the D-learning method is able to eliminate a large proportion of unwanted rules causal forest generates.

3.2.3. Rule analysis

Interpreting our estimated $\tau(X)$ relies on understanding the subgroups contributing to it. A comprehensive analysis of the subgroups identified is what needs to be improved in existing studies. This analysis is indispensable since i) we cannot guarantee that all the rules D-learning selects have their stated impact on our estimators, and ii) the size of the rules may still be too large to achieve human comprehension. Thus, we show a procedure to further analyze the rules remaining in the candidate set to find a relatively smaller yet more promising subset of rules. For clarification, this procedure continues to remove a large number of rules, primarily to enhance interpretability, and the estimation of ITE is still made on all the rules D-learning selects (rules with non-zero weights). This procedure includes but is not necessarily limited to the following three parts: overall analysis, rule significance analysis, and rule decomposition analysis. Unlike previous studies, our analysis does not focus on the subgroups with higher treatment effects but on those with significantly different ITE estimates, whether higher or lower.

Overall analysis. Suppose D-learning selects a rule set that consists of n_1 rules ($n_1 \leq M$) whose weights are non-zero in model (5), i.e., $\hat{R}_1 = \{\hat{r}_1, \hat{r}_2, \dots, \hat{r}_{n_1}\}$ (for simplicity, we use \hat{r}_j instead of $\hat{r}_j(x)$ to represent a rule). The corresponding CRL estimates of ITE $\hat{\tau}_{CRL}$ are also obtained based on this rule set. As estimation accuracy is the basis of interpretability, the overall analysis aims to evaluate how this rule set collectively performs on ITE estimation using various performance metrics. For simulated data where the true treatment effect is already known, we define Mean Squared Error (MSE), Mean Potential Outcomes (MPO) and Population Overlap (PO) to evaluate and compare our estimator with other baselines. For observational data where the ground truth can never be observed, the above metrics can no longer be used, so we use ITE-based prediction accuracy, Empirical Expected Outcome (EEO)

and Treatment Efficient Frontier. Details of these metrics can be found in section 4.1 for simulated data and 4.2.2 for real-world data.

Suppose the above overall analysis shows that our method is able to give comparable ITE estimates to that of baseline methods, we then continue the following analysis, which evaluates each rule in terms of i) the ability to distinguish different levels of ITE, i.e., rule significance, and ii) the role of each component in the rule, i.e., rule decomposition analysis.

Rule significance analysis. A rule defines two subpopulations: the population that satisfies the rule $G^Y = \{i|r(X_i) = 1\}$ and the rest that does not $G^N = \{i|r(X_i) = 0\}$. Therefore, we want to test the discriminating power of a rule by checking if G^Y and G^N differ significantly in the magnitude of ITE estimates, using the well-known two-sample Kolmogorov–Smirnov test [7]. This test is commonly used to determine whether two samples originate from the same continuous distribution. In our context, the null hypothesis posits that the ITE estimates for groups G^Y and G^N derive from an identical distribution. If the null hypothesis cannot be rejected, we assume there is no significant difference in the ITE estimates between the two groups. Specifically, a p -value ≤ 0.05 implies that the rule can identify a subgroup with significantly different treatment effects than the rest of the population. We perform this test on each rule in \hat{R}_1 and remove those with p -value > 0.05 . The remaining n_2 rules ($n_2 \leq n_1$) form the new candidate rule set \hat{R}_2 .

Rule decomposition analysis. Decomposition analysis evaluates how each component in a rule contributes to the complete rule in differentiating treatment effect. For example, if we have a rule \hat{r}_j that has three components a , b and c , we can derive three revised rules: \hat{r}_j^a , \hat{r}_j^b and \hat{r}_j^c . \hat{r}_j^a is the rule with component a removed from the original rule, that is, the rule formed only by component b and c and similarly for \hat{r}_j^b and \hat{r}_j^c . We do the above significance analysis on all revised rules and obtain their corresponding p -values p_j^a , p_j^b and p_j^c . We think a higher p -value of the revised rule than that of the original complete rule, say, $p_j^c > p_j$, implies that the revised rule \hat{r}_j^c is less significant in distinguishing subpopulations with different levels of ITE estimates than the original entire rule \hat{r}_j . Hence, the removed component c contributes to the significance of the ITE difference. The higher the p -value of the revised rule, the more critical the variable being removed is, which reveals the variable most accountable for the group’s heterogeneity. In contrast, a lower value suggests the corresponding component(s) may be unnecessary and meaningless to the complete rule since its removal does not reduce the significance of the difference but increases it. Therefore, if all revised rules have higher p -values ($p_j < \min\{p_j^a, p_j^b, p_j^c\}$), then all the components in the rule work synergistically to contribute to its discriminating power. In this step, we retain the rules that have higher p -values on all the corresponding revised rules to form a new refined set \hat{R}_3 with n_3 rules ($n_3 \leq n_2$).

The rule analysis step shows a universal way to analyze the identified rules through different levels. However, these tools highly rely on the data in hand. Therefore, we highly recommend using this analysis procedure as a screening step for the lengthy list of rules and picking out the top subgroups for more rigorous statistical test and further interpretation.

Our whole workflow helps us to estimate and build a better understanding of HTE for complex diseases by finding potential subgroups of heterogeneity and exploring the relationship between ITE and CATEs of these subgroups. Take Figure 1 as an example, the rule discovery step first identifies a large pool of interpretable rules as candidate subgroups. The rule selection process then removes a great proportion of

non-informative and fake subgroups from the candidate set and uses the remaining M subgroups as the selected sources of effect heterogeneity to learn the connection between ITE and subgroup CATEs (through τ and β). Finally, the rule analysis part evaluates how accurate these M subgroups estimate ITE as a whole and looks deeper into each of the M subgroups to evaluate how each subgroup and the factors involved in the subgroup contributes to HTE estimation.

4. Evaluation of CRL Performance

In this section, we use both simulated data and real-world data to evaluate how well CRL performs in estimating and providing insights to HTE. Specifically, the simulated RCT data is mainly performed to evaluate the estimation accuracy of CRL while the real-world application demonstrates how to apply CRL in observational data and how CRL gives insights to us on real-world problems (enhanced understanding). In addition, we also compare CRL with several previously mentioned baseline methods, namely outcome weighted estimation (OWE) [50], causal tree (CT) [3], causal forest (CF) [45], patient rule induction method (PRIM) [9] and causal rule ensemble (CRE) [28] in both the simulation experiments and real-world applications. Baseline methods are implemented with R package *personalized* [24] for OWE (linear), *causalTree* [4] for causal tree, *subgrpID* [22] for PRIM, *grf* [40] for causal forest.

4.1. Simulation study

4.1.1. Data setups

To evaluate how well CRL performs in estimating HTE, we first generate simulated RCT data sets $\{X_i, A_i, Y_i\}_{i=1}^N$ based on assumption (2) with varying configurations. Specifically, we generate covariates $X \in \mathbb{R}^9$ where the first three elements (features) x_1, x_2 , and x_3 are randomly drawn from $\{0, 1\}$ with equal probability (x_3 is sampled differently for some setups of the true group, shown later). The last six features are $\{x_j | j = 4, 5, \dots, 9\} \stackrel{\text{i.i.d.}}{\sim} \mathcal{N}(0, 2)$. For simplicity, we ignore the sample subscript notation i , and the remaining subscript represents certain features unless otherwise noted. The baseline effect is defined as $f(X) = 1 + x_1^2 + 3x_1x_6 + 0.4x_4x_7 + x_5 - x_6 + 0.5x_3x_8$. Based on (2), we can define any number of true subgroups and their related true CATEs via a rule form (shown later). Once we set the true $\tau(X)$, we define the potential outcomes for both the negative and positive treatments: $Y(-1) = f(X) + \epsilon$ and $Y(1) = Y(-1) + \tau(X)$, where $\epsilon \sim \mathcal{N}(0, 1)$. We imitate the simplest RCT assignment of the treatment arm: A_i is sampled from $\{-1, 1\}$ with equal probability. Therefore, the observed outcome in our data set is $Y_i = 2^{-1}(1 + A_i)Y_i(1) + 2^{-1}(1 - A_i)Y_i(-1)$.

To sum up, the observed data set $\{X_i, A_i, Y_i\}_{i=1}^N$, together with the predefined baseline effect $\{f(X_i)\}_{i=1}^N$ and true ITE $\{\tau(X_i)\}_{i=1}^N$ forms the basis of the ground truth of the data generation. To avoid randomness and to test how the performance of CRL changes with the data settings, we make a few variations to our simulated data:

- Number of the observations (num.obs) $N \in \{2500, 5000, 10000\}$,
- Effect size base quantity $k \in \{5, 10, 15, 20, 25, 30\}$, where k is used in the definition of true subgroups and related τ in Figure 3.
- Number of true positive subgroups (num.grp) defined in rules: $M^* \in \{1, 3, 5\}$. If $M^* = 5$, $x_3 \sim U(0, 10)$, otherwise, it still follows the before-mentioned Bernoulli

num.grp = 1		
x_1	x_2	τ
1	1	k
0	0	-k
otherwise		0

num.grp = 3			
x_1	x_2	x_3	τ
1	0	0	k
1	1	0	2k
1	1	1	3k
0	0	0	-k
otherwise			0

num.grp = 5			
x_1	x_2	x_3	τ
1	1	>5	3k
0	1	>5	2k
1	0	>5	
1	1	≤ 5	
0	0	>5	k
0	0	≤ 5	-k
otherwise			0

Figure 3. Specification of true treatment effect $\tau(X)$ for varying numbers of subgroups. k is the effect size base quantity and τ is the true treatment effect. For each scenario, once k is given, we set τ to different multiples of k depending on the covariates. E.g., for num.grp = 3, $\tau = k$ if $x_1 = 1, x_2 = 0$ and $x_3 = 0$ whereas $\tau = 2k$ if $x_1 = 1, x_2 = 1$ and $x_3 = 0$.

distribution. For a clearer performance comparison, we focus on identifying subgroups whose true treatment effects are positive (i.e., true positive subgroups), which most baseline methods only care about. However, we keep the pre-defined negative groups in our setups.

Together, we have $3 \times 3 \times 6 = 54$ data sets. We first make 100 re-sampled repetitions for each data set and randomly split each repetition into a 70% training set and 30% test set. Then, we apply the overall CRL workflow as well as other baseline methods on the training data and report performance on the test data, averaging over 100 repetitions.

4.1.2. Performance metrics for method evaluation

Performance metrics used in this study focus on how accurately a method estimates ITE. To evaluate so, we use Mean Squared Error (MSE), i.e., $MSE(\hat{\tau}) = N^{-1} \sum_{i=1}^N (\hat{\tau}(X_i) - \tau(X_i))^2$, where $\hat{\tau}(X_i)$ and $\tau(X_i)$ are a certain estimate and the true ITE of instance i respectively. The smaller the value, the better an estimator does. Besides MSE, we also evaluate performance from two other supplementary perspectives, namely Mean Potential Outcomes (MPO) and Population Overlap (PO).

MPO, defined as $N^{-1} \sum_{i=1}^N Y_i(d(X_i))$, measures how good the average outcomes can be under a certain treatment assignment strategy $d(X)$. The larger the value of MPO, the better the treatment strategy is. For an intuitive comparison, we use the simplest strategy that the treatment recommendation is purely based on the sign of ITE estimates, i.e., $d(X_i) = 1$ if $\hat{\tau}(X_i) > 0$ and -1 otherwise.

We define $PO = |T \cap I| / |T \cup I| \in [0, 1]$ where $T = \{i \in N | \tau(X_i) > 0\}$ and $I = \{i \in N | \hat{\tau}(X_i) > 0\}$ represent respectively the sets of instances whose true ITE and estimated ITE are positive and $|\cdot|$ is the number of instances in a set. This measure evaluates the degree of intersection of the two sets. When $T \cap I = \emptyset$, $PO = 0$ and when $T = I$, $PO = 1$. Larger values are preferred.

We also use the above metrics for tuning the parameters involved in CRL and other methods. Please see Appendix C for details.

4.1.3. Simulation results

This section shows the results of the performance comparison between CRL and other baseline methods for each of the 54 data sets (setting). Since the baseline methods vary in research focus and model outputs, not all methods can be directly compared. Specifically, CT, CF, OWE and CRL are able to give ITE estimates for every instance in the data, so we compare and show their estimation accuracy on the whole population in Figure 4. For CRE and PRIM, which only identify specific subpopulations with enhanced treatment effect, we compare them with CRL only on the subgroups they respectively identify, shown in Figure 5

Figure 4(a) shows the comparison of MSE between CT (blue), CF (green), OWE (yellow), and CRL (black). For panels from the top to bottom, the number of observations of the data set varies from 2,500 to 10,000, and from left to right, the number of true positive subgroups varies from one to five. Effect size (k) is reflected in the x-axis and each value shown is an average of 100 runs on the specific setting. Figure 4(b), 4(c), 4(d), 5(a) and 5(b) are presented in the same way as Figure 4(a) for other metrics.

Figure 4(a) shows that each method’s MSE increases as the effect size grows across different configurations. In general, CRL is almost always among the best performers across all settings. For cases where $num.true.grp = 1$, CT, CRL, and OWE have almost the same performance. Hence their curves overlap. Obviously, the superiority of CRL increases gradually as the number of observations and true subgroups increase under large effect sizes (e.g., $k \in \{20, 25, 30\}$). Besides, from Figure 5, we see that no matter for the subgroups identified by CRE (pink) or PRIM (red), CRL has consistently much lower MSE, indicating that CRL performs better for treatment effect estimation of complex diseases which have many potential contributing factors and interactions between these factors. In contrast, both CRE and PRIM identify a limited number of subgroups (most of the time they only identify one single subgroup) and variables, failing to achieve the goal.

Figure 4(b) compares how well the involved methods do in treatment recommendations using MPO. CRL, CT, and CF show almost the same good performance on MPO and outperform OWE in all settings. The identical performance of the former three methods is a result of our treatment assignment strategy: We recommend treatment based solely on the sign of ITE estimates. Regardless of how these methods differ in the magnitude of the estimates, they yield identical treatment recommendations as long as their estimates have identical signs, hence the same values on MPO. Figure 4(c) shows that CRL has comparable performance to baseline methods with regard to PO across most settings (with higher overlap value and lower variance), indicating that it is able to recover the majority of populations with positive treatment effect.

Since CRL filters out rules from the original rule set generated by CF, we also compute the proportion of CF rules filtered out by CRL, i.e., $1 - W_{CRL}/W_{CF}$ where $W_{CRL} = |\{r_m | r_m \in I_{CRL}, r_m \notin T\}|$ represents the number of fake rules in the rule set (I_{CRL}) identified by CRL, and W_{CF} represents the same for CF. The bigger the value, the better CRL filters out fake rules. As indicated in Figure 4(d), through the additional D-learning selection and rule analysis procedure, CRL is able to filter out a high proportion of fake rules CF generates.

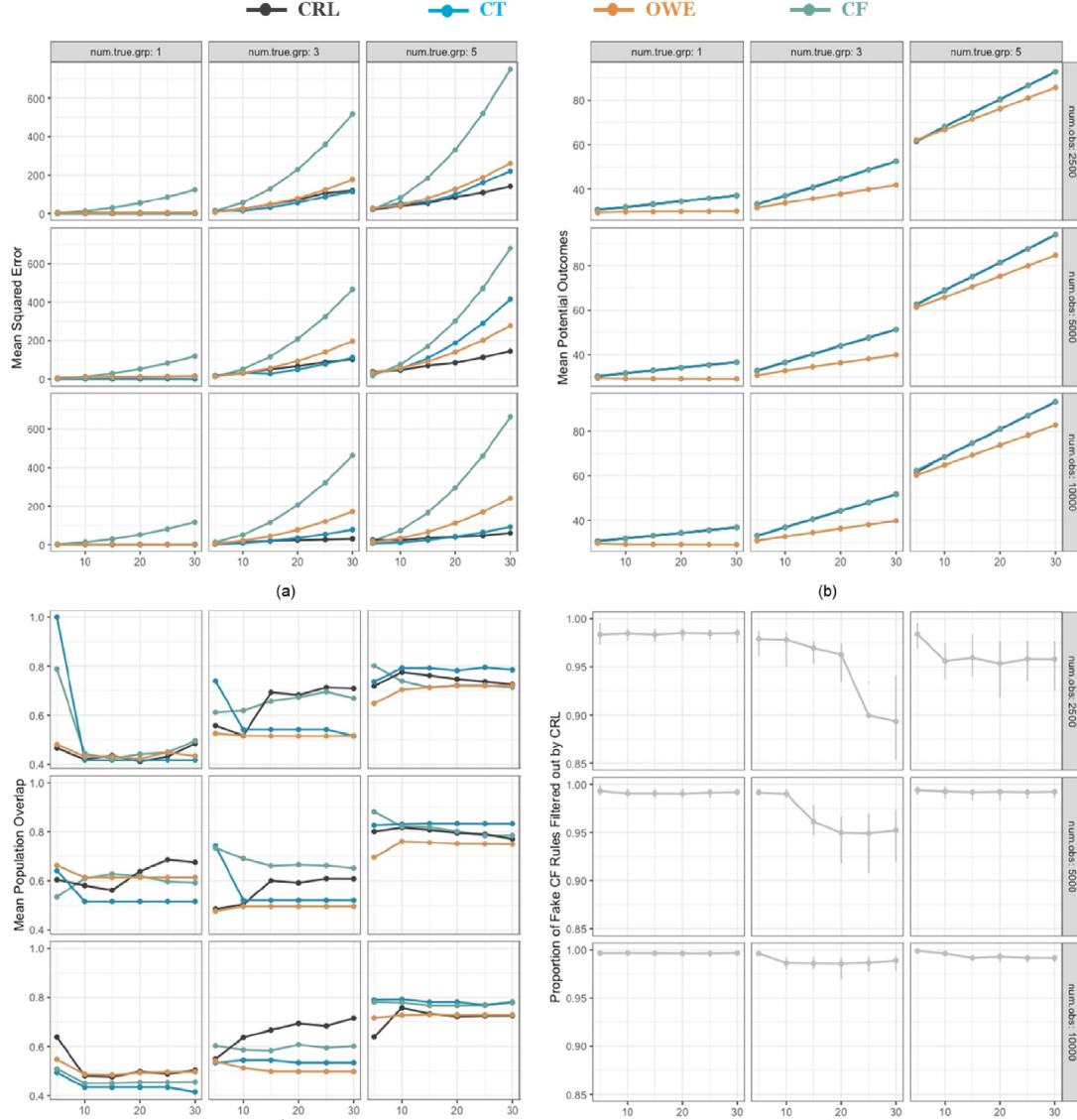


Figure 4. Performance comparison of CRL (black) and baseline methods CT (blue), CF (green), OWE (yellow) applied on the simulated data. All performance metrics are averaged over 100 repetitions for each data set. (a) Mean squared error of treatment effect. (b) Mean potential outcomes. Note that CRL, CT and CF have identical performance on MPO, hence their curves overlap. (c) Mean population overlap. (d) Proportion of fake CF rules filtered out by CRL.

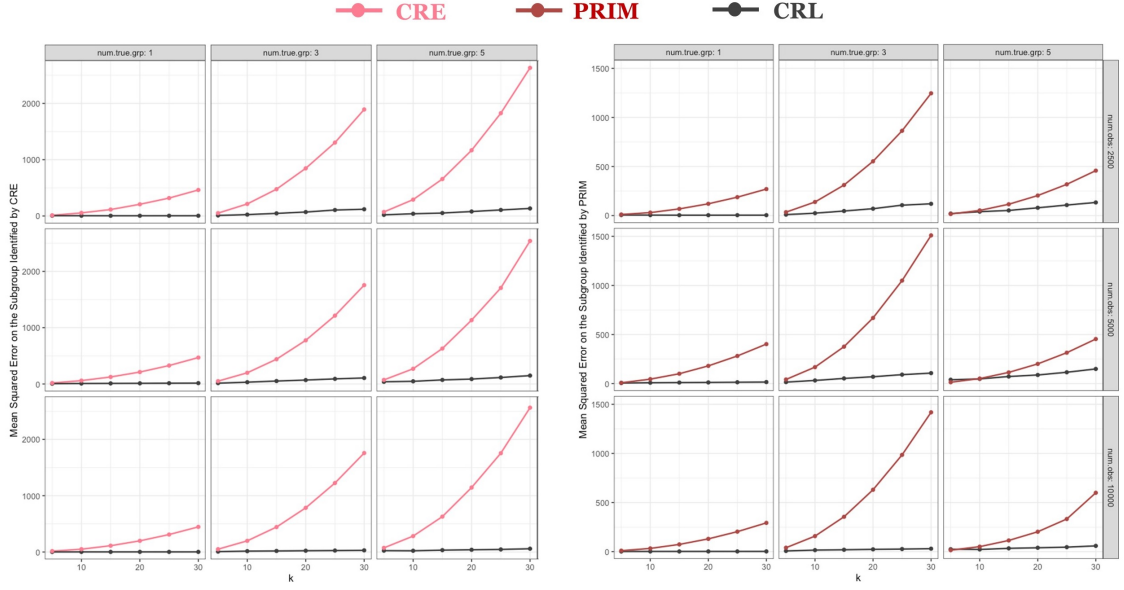


Figure 5. Comparison of mean squared error of treatment effect on specific subpopulations between CRL and baseline methods CRE (pink) and PRIM (red) applied on the simulated data. Each value shown is the average over 100 repetitions for each data set. (a) MSE of CRL versus CRE on the subgroup identified by CRE. (b) MSE of CRL versus PRIM on the subgroup identified by PRIM.

4.2. Real-world data application

In this part, we apply the CRL workflow to atrial septal defect (ASD) data to demonstrate its usage and performance (especially interpretability) in real-world observational data. ASD is a congenital heart defect characterized by a hole in the wall (atrial septum) that separates the upper chambers (atria) of the heart. As a common type of birth defect, ASD has a prevalence of 2.5 out of 1000 in live births and 25% to 30% present in adulthood [8, 43].

In this study, we focus on two common ASD treatments: percutaneous interventional closure (PIC) and minimally invasive surgical closure (MISC). PIC involves using catheters to reach the heart through blood vessels and repair the defect with an occluder, while MISC involves making a small incision in the chest, allowing access to the heart for patching. We investigate the HTE of PIC versus MISC (negative treatment) on hospital-free days within one year after discharge (HFD1Y). Hospital-free days are the days patients spend outside of the hospital. Instead of *survival* or *alive days* that overemphasize the survival goal, it is more pragmatic and patient-centered, reflecting more information on patient’s quality of life [6].

In what follows, we first briefly introduce the ASD data. Then, we list a few performance metrics designed particularly for HTE estimation in real-world data where the ground truth of the treatment effect and the treatment assignment mechanism are unknown. Finally, we show the performance comparison of CRL and other baseline models on estimation accuracy and enhanced understanding of ITE. Note that all the CRL rules mentioned and presented in the following text have already been screened through the rule analysis process.

4.2.1. Overview of the ASD data

The ASD data used in this study is extracted from congenital heart disease data collected from thirteen clinical centers in China with the initiative to analyze and compare clinical pathways for first-surgery patients (patients undergoing surgery for the first time). The data includes 6780 patient records with 250 variables, spanning from hospital admission and preoperative examination to diagnoses, surgery, discharge, and follow-up visits. To implement our analysis, we extract the records of patients who were diagnosed with only ASD and treated with either PIC or MISC. There are only 1.16% missing values in these records, so we simply impute the data with K-Nearest Neighbor (number of neighbors set to 10). The final data includes 2850 observations, with 16 pre-treatment variables and five surgery-related variables, some of which are manually integrated with multiple original variables to make the variable set more concise. Pre-treatment variables include the information generated on admission, through the inquiry and diagnosis, and from pre-surgery medical check results. For instance, on admission, we have: i) two cumulative scores on disease history *chdhis* and *othdhis*. If a patient's *chdhis* = 3, it means that the patient has three previous cardiovascular conditions, ii) basic measurements with *sysbp* and *diabp* representing systolic and diastolic blood pressure respectively, and *BMI* the Body Mass Index, and iii) demographic information like age and *sex*.

We give details of the ASD data in Appendix D where Figure D1 shows the variable details and Table D1 and Table D2 show the descriptive statistics for the pre-treatment variables and the surgery-related variables (and outcome HFD1Y), respectively.

Before we apply CRL to this observational data, we first need to pre-process the data using the propensity score matching method [49], which has proven to be very useful in estimating treatment effects using observational data [2]. This process allows us to match the data samples from both treatment groups to achieve pseudo randomization of treatment assignment and to overcome the unsatisfactory overlap between two groups, thus ensuring the satisfaction of the unconfoundedness assumption and overlap assumption. Additionally, this process models propensity scores that can be used in the D-learning step. Details of the matching process can be found in Appendix E, after which 26 observations are eliminated from the data and variable *atsize0* is replaced by its square root, *sq.atsize0* for better covariate balance. We then use the matched data from this process to fit all models for performance evaluation.

4.2.2. Performance metrics for real-world observational data

When estimating the treatment effect using real-world data, the ground truth is never known. Thus, we can no longer use the performance metrics defined for simulated data. Instead, we have to do so in some indirect ways based on what we know, like the following shown:

i) ITE-based prediction accuracy. It is reasonable to evaluate the potential accuracy of ITE estimation based on the prediction accuracy of known observed outcomes Y . Consider $Y(-1) = f(X) + \epsilon$ which merely reflects the baseline effect and $Y(1) = Y(-1) + \tau(X)$. Then for the same outcome prediction model $\hat{Y} = g(\hat{\tau}(X), x)$ using entirely the same variables x but different ITE estimates $\hat{\tau}(X)$, the difference in prediction accuracy, say $MSE(g(\hat{\tau}(X)))$ mainly comes from the difference in $\hat{\tau}(X)$. Hence, in general, the method that predicts the outcome better (lower MSE) estimates $\tau(X)$ better.

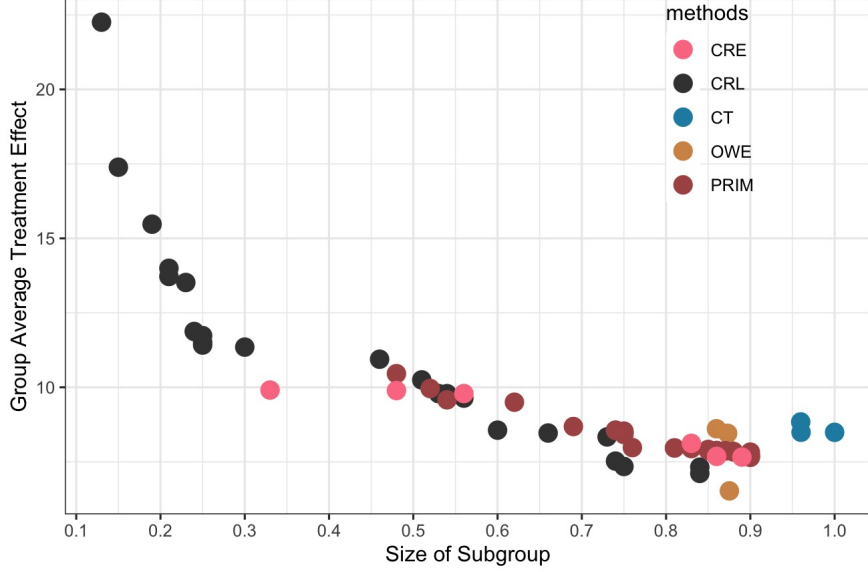


Figure 6. Treatment efficient frontiers of all methods fit for 100 repetitions

ii) Empirical expected outcome (EEO). This metric is defined in [34] as:

$$\hat{V}(d) = \frac{\mathbb{E}_n[Y1(A = d(X))/\pi(A, X)]}{\mathbb{E}_n[1(A = d(X))/\pi(A, X)]},$$

where \mathbb{E}_n denotes empirical average and $d(X)$ denotes a specific personalized treatment strategy that maps a given X to a certain treatment. This metric, in essence, measures the mean magnitude of the observed outcomes Y that a treatment strategy achieves when its treatment recommendations align with the treatments actually received by the samples. The higher this expected outcome, the better the treatment strategy is, and implicitly, the more accurate our ITE estimation is.

iii) Treatment efficient frontier, proposed in [47], is a graphic comparison of subgroups obtained from different methods, given that the identified subgroups differ in group size (proportion of samples) and CATE. Though not always the case, a small group usually has a higher CATE than a bigger one, so it is hard to tell which subgroup is better. To balance the trade-off between subgroup size and subgroup CATE, the authors define the concept of treatment efficient frontier, which is formed with all dominant groups (subgroup that has no other subgroup surpasses it in both size and CATE) a certain method identifies. This frontier is then mapped to the two-dimensional coordinate system with the x -axis being the size and y -axis the CATE estimates of the dominant groups. With this graph, we can see how quickly the estimated treatment effect magnitude decays as the subgroup covers more samples and easily spot the method that has the highest frontier since they find subgroups with larger sizes and CATE. See Figure 6 for example.

Considering the above performance metrics, especially the ITE-based prediction accuracy, we implement all methods: We first split the ASD data into three parts: 40% (estimation set) for ITE estimation with all methods; 40% (prediction set) for outcome prediction using the least squares model (or any other proper prediction models) fed with all the same variables except the different ITE estimated by different

Table 1. Mean squared error (MSE) and empirical expected outcome (EEO) averaged on 100 repetitions of ASD data applying CRL and other baseline models. SD is the standard deviation of MSE and EEO.

	Mean MSE (SD)	Mean EEO (SD)
CRL	21.608 (12.840)	360.514 (0.763)
CF	21.619 (12.844)	360.732 (0.338)
CT	22.513 (13.817)	359.729 (0.281)
OWE	21.582 (12.831)	360.569 (1.042)
PRIM	21.622 (14.541)	359.691 (0.323)
CRE	21.112 (14.001)	359.062 (1.154)

Table 2. Eight CRL subgroups that most impact the estimates of treatment effect, displayed in descending order of the absolute value of the subgroup CATE multiplied by the subgroup weight.

Subgroup	CATE	Weight	CATE × Weight
BMI>14.4 and electb=1 and oroom=1 and othchd>0	2.92	119.54	349.44
age≤9 and age>5	7.62	-42.42	-323.34
age>8 and NYHA≤1	5.98	50.70	303.11
age>7 and NYHA≤1 and sq.atsize0≤4.8	7.09	-42.64	-302.33
murmur≤2 and sysbp>100	7.79	-31.14	-242.45
age>5 and BMI>17.2 and electb=1	6.09	-38.38	-233.79
age>15 and BMI>13.7	6.85	-33.52	-229.63
diabp>59 and electb=1 and oroom=0	6.80	29.20	198.66

methods in the previous step. The remaining 20% data (test set) is used to report the first two performance metrics, i.e., $MSE(g(\hat{\tau}(X)))$ and EEO.

We repeat the above procedure 100 times with randomly re-sampled ASD data and tune the parameters using the same approach as in the simulation part. See Appendix C for details.

To evaluate treatment efficient frontier, we use the entire data to fit all models for each of the re-sampled data, since CRL generally needs more observations to discover potential subgroups. For each method to be compared, we pool the subgroups identified from all 100 repetitions together and find its dominant subgroups, which form the ultimate frontier.

4.2.3. Model results and interpretation

We list the MSE of the predicted HFD1Y and EEO of all methods averaged over 100 repetitions in the first and second rows in Table 1. It is obvious that all methods show similar accuracies of outcome prediction (MSE) and recommendation performance (EEO) on the ASD data. Figure 6 shows the treatment efficient frontier of all methods. Obviously, compared with other methods, CRL identifies subgroups with a variety of sizes ranging from 0.1 to 0.85 and effect sizes ranging from 4 to 25. In contrast, methods like OWE and CT, only identify big subgroups with relatively small subgroup CATE. Note that we do not show the frontier of CF in this figure as it overlaps with the frontier of CRL whose dominant groups are part of CF groups.

The above results demonstrate that CRL achieves at least comparable results against baseline methods in ITE estimation and subgroup identification on the ASD data. Moreover, it provides us with an enhanced understanding of ITE of ASD treatments on HFD1Y through the contributing informative rules we learned from the whole workflow.

For a concise presentation of what we learned from the ASD data with CRL, we list the eight rules that impact the estimated treatment effect the most in a randomly chosen rule set out of the 100 rule sets, with their corresponding CATE estimates and learned weights (See Table 2). The rules are displayed in decreasing order of the absolute value of the signed product of subgroup CATE multiplied by subgroup weight. For example, the first rule means that when a patient with abnormal ECG result, BMI>14.4, othchd>0 and is operated at a one-stop operating room, the patient’s ITE of PIC against MISC will increase by 349.44 days. However, this estimate will then decrease by 323.34 if the patient’s age is between five and nine. The final ITE estimate of a patient is the summation of all the products corresponding to the subgroups a patient belongs to, showing how a patient’s ITE is affected by the combination of potential rules.

These eight rules identify several important factors, such as age, BMI, electb, oroom, and NYHA, with meaningful cut-off value (e.g., 14.44 for BMI), influencing the treatment effect of PIC versus MISC on HFD1Y. Age and BMI are the two most involved factors in the rules, indicating they play indispensable roles in the way HFD1Y is affected by PIC and MISC. This is consistent with [23] and [33] stating that age and weight-related factors like BMI are particularly important in surgery decisions and the prognosis of ASD, such as length of hospital stay. Compared to MISC, PIC, in general, has the advantage of shorter hospital stay and is more suitable for non-underweight children or older children [33], which is reflected with the HFD1Y increase in the first (BMI>14.4) and second rule (age>8). For children aged between five and nine (second rule), the decrease of HFD1Y or the increase in hospital stay, may be due to a lower percentage of PIC-treated patients within the group compared to that of the remaining population (81% versus 85%). This reveals the preference for MISC against PIC in the young-aged group, which has been a fact in past ASD treatment practices [27].

In addition, these rules identify multiple cut-off values for the same factors, such as age with thresholds at 8 (third rule) and 15 (seventh rule), together with NYHA and sq.atsize0, revealing potential complex interactions between these factors. Although there is little evidence of these interactions, we believe they enlighten people in the community on new research directions, such as designing rigorous experiments to further validate these underlying relationships. We also list the details of the dominant

Table 3. The dominant subgroups identified by CRE, displayed in descending order of subgroup CATE.

Subgroup	CATE	Size
othchd>0 and sq.atsize0>0 and electb≤0	9.91	0.33
atrial>2 and electb≤0	9.89	0.48
atrial≤2 and electb≤0	9.79	0.56
mesh≤0 and BMI≤22	8.12	0.83
atrial=2	7.68	0.86
chdhis≤2 and sq.atsize0>0 and BMI≤22	7.66	0.89

subgroups of CRE (See Table 3) and PRIM (eight top rules by subgroup CATE, see Table 4) shown in Figure 6 for a better comparison on interpretability. Apparently, both CRE and PRIM identify relatively homogeneous rules that entail limited information. We find that for the same variable (except murmur), its cutoff value is almost the same in all the rules involved, such as 2 for atrial, NYHA and chdhis across all rules. Many rules share similar and even identical variables, such as atrial>2 and electb≤0, atrial≤2, and electb≤0 (the second and third rules) in Table 3 and the first two rules in Table 4, which further exacerbates this rule of homogenization. As a result, the

Table 4. The eight top dominant subgroups identified by PRIM, displayed in descending order of subgroup CATE.

Subgroup	CATE	Size
NYHA ≤ 2 and othdhis ≤ 0 and occnum ≤ 1 and chdhis ≤ 2 and atrial ≤ 2 and mesh ≤ 0 and othchd ≤ 5 and surgesitua ≤ 1 and murmur ≥ 3	10.46	0.48
NYHA ≤ 2 and chdhis ≥ 1 and chdhis ≤ 2 and surgesitua ≤ 1 and occnum ≤ 1 and atrial ≤ 2 and othdhis ≤ 0 and mesh ≤ 0 and oroom ≤ 0 and murmur ≥ 2	9.96	0.52
chdhis ≤ 2 and NYHA ≤ 2 and murmur ≥ 3	9.59	0.54
NYHA ≤ 2 and occnum ≤ 1 and chdhis ≤ 2 and othdhis ≤ 0 and mesh ≤ 0 and surgesitua ≤ 1 and murmur ≥ 2	9.50	0.62
oroom ≤ 0 and NYHA ≤ 2 and chdhis ≥ 1 and occnum ≤ 1 and chdhis ≤ 2 and othchd ≤ 5 and mesh ≤ 0 and atrial ≤ 2 and othdhis ≤ 0	8.68	0.69
oroom ≤ 0 and occnum ≤ 1 and NYHA ≤ 2 and atrial ≤ 2	8.56	0.74
NYHA ≤ 2 and oroom ≤ 0 and atrial ≤ 2	8.55	0.74
NYHA ≤ 2 and chdhis ≤ 2 and chdhis ≥ 1 and oroom ≤ 0	8.53	0.75
NYHA ≤ 2 and surgesitua ≤ 1 and oroom ≤ 0	8.48	0.75
surgesitua ≤ 1 and oroom ≤ 0	8.42	0.75

subgroups identified are highly overlapping, hence the estimates of their treatment effects are also quite close. In contrast, CRL can explore a more diverse combination of variables for potential relationships in the ASD data. When different variables interact with each other, CRL identifies different cut-off values for each variable, which is more in line with the actual situation of complex disease, therefore providing much more interpretation and insights to healthcare practitioners.

5. Conclusions and future work

This study introduces a rule-based framework, CRL, aimed at enhancing our understanding of HTE estimation for complex disease treatment in clinical scenarios. CRL leverages causal forest to discover a pool of potential rules for ITE estimation (rule discovery) and then utilizes the D-learning method to filter out non-informative rules, imposing sparsity on the rules (rule selection). By deconstructing the estimated ITE through a weighted combination of the informative rules selected by D-learning, CRL explores HTE with a novel perspective that connects group-level and individual-level treatment effects. The understandable rules, their corresponding CATE estimates, weights in combination, and the comprehensive procedure for evaluating each causal rule from multiple perspectives (rule analysis) together give insights into the treatment of a complicated disease. The remaining rules that survive after the rule analysis step may reveal potential meaningful interactions between involved variables, paving the way for further investigation and validation.

This research has several methodological limitations that could be addressed in future studies. First of all, CRL requires the outcome of interest be continuous and prefer higher values. Treatment in our study is also limited to the binary case. These limits hinder the wide application of the method in healthcare practice. Secondly, our assumption of ITE is based on a linear combination of potential rules for simplicity, while the non-linear case is not discussed. Last but not least, in the evaluation of CRL from treatment recommendation, we simply recommend treatments based on the sign of the estimated ITE and do not consider the cost-sensitive scenarios where treatment resource are constrained. Future work may introduce more economic factors and explore how to better estimate treatment effects and recommend treatments in complex scenarios.

Conflicts of Interest

The authors declare no conflicts of interest.

Data Availability Statement

The data that support the findings of this study contain sensitive patient information and, therefore, cannot be made publicly available. However, these data are available from the corresponding author upon reasonable request, subject to appropriate confidentiality agreements.

References

- [1] A. Alaa and M. Schaar, *Limits of estimating heterogeneous treatment effects: Guidelines for practical algorithm design*, in *International Conference on Machine Learning*. PMLR, 2018, pp. 129–138.
- [2] H.C. Ankarali, V. Sumbuloglu, A.C. Yazici, I. Yalug, and M. Selekler, *Comparison of different matching methods in observational studies and sensitivity analysis: The relation between depression and stai-2 scores*, *EXPERT SYST APPL* 36 (2009), pp. 1876–1884. Available at <https://www.sciencedirect.com/science/article/pii/S0957417407006343>.
- [3] S. Athey and G. Imbens, *Recursive partitioning for heterogeneous causal effects*, *Proc Natl Acad Sci* 113 (2016), pp. 7353–7360.
- [4] S. Athey, G. Imbens, and Y. Kong, *Recursive Partitioning Causal Trees* (2016). Available at <https://github.com/susanathey/causalTree>, R package version 0.0.
- [5] S. Athey, J. Tibshirani, and S. Wager, *Generalized random forests*, *Ann Stat* 47 (2019), pp. 1148–1178.
- [6] C.L. Auriemma, S.P. Taylor, M.O. Harhay, K.R. Courtright, and S.D. Halpern, *Hospital-free days: A pragmatic and patient-centered outcome for trials among critically and seriously ill patients*, *Am J Respir Crit Care Med* 204 (2021), pp. 902–909.
- [7] V.W. Berger and Y. Zhou, *Kolmogorov–smirnov test: Overview*, Wiley Statsref: Statistics Reference Online (2014).
- [8] M. Brida, M. Chessa, D. Celermajer, W. Li, T. Geva, P. Khairy, M. Griselli, H. Baumgartner, and M.A. Gatzoulis, *Atrial septal defect in adulthood: a new paradigm for congenital heart disease*, *Eur Heart J* 43 (2021), pp. 2660–2671.
- [9] G. Chen, H. Zhong, A. Belousov, and V. Devanarayan, *A PRIM approach to predictive-signature development for patient stratification*, *Stat Med* 34 (2015), pp. 317–342.

- [10] S. Chen, L. Tian, T. Cai, and M. Yu, *A general statistical framework for subgroup identification and comparative treatment scoring*, Biometrics 73 (2017), pp. 1199–1209.
- [11] Z. Chen and J. Xie, *Estimating heterogeneous treatment effects versus building individualized treatment rules: Connection and disconnection*, Statistics & Probability Letters 199 (2023), p. 109854.
- [12] J. Crabbé, A. Curth, I. Bica, and M. van der Schaar, *Benchmarking heterogeneous treatment effect models through the lens of interpretability* (2022). Available at <https://arxiv.org/abs/2206.08363>.
- [13] R. Dwivedi, Y.S. Tan, B. Park, M. Wei, K. Horgan, D. Madigan, and B. Yu, *Stable discovery of interpretable subgroups via calibration in causal studies*, Int Stat Rev 88 (2020), pp. S135–S178.
- [14] S. Feng, K. Kong, Y. Kong, G. Li, and Z. Wang, *Statistical inference of heterogeneous treatment effect based on single-index model*, Comput Stat Data Anal 175 (2022), p. 107554.
- [15] J.C. Foster, J.M. Taylor, and S.J. Ruberg, *Subgroup identification from randomized clinical trial data*, Stat Med 30 (2011), pp. 2867–2880.
- [16] J. Friedman and B. Popescu, *Predictive learning via rule ensembles*, Ann Appl Stat 2 (2008), pp. 916–954.
- [17] A. Hapfelmeier, K. Ulm, and B. Haller, *Subgroup identification by recursive segmentation*, J APPL STAT 45 (2018), pp. 2864–2887.
- [18] Y. He, G. Huang, S. Chen, J. Teng, K. Wang, Z. Yin, L. Sheng, Z. Liu, Y. Qiao, and J. Shao, *X-Learner: Learning Cross Sources and Tasks for Universal Visual Representation*, in *Computer Vision–ECCV 2022: 17th European Conference*. Springer, 2022, pp. 509–528.
- [19] Y. He, S. Kim, M.O. Kim, W. Saber, and K.W. Ahn, *Optimal treatment regimes for competing risk data using doubly robust outcome weighted learning with bi-level variable selection*, Comput Stat Data Anal 158 (2021), p. 107167.
- [20] A. Herlitz, *Comparativism and the grounds for person-centered care and shared decision making*, J Clin Ethics 28 (2017), pp. 269–278.
- [21] D.E. Ho, K. Imai, G. King, and E.A. Stuart, *MatchIt: Nonparametric preprocessing for parametric causal inference*, J Stat Softw 42 (2011), pp. 1–28.
- [22] X. Huang, Y. Sun, and S. Chatterjee, *SubgrpID: Patient Subgroup Identification for Clinical Drug Development* (2017). Available at <https://CRAN.R-project.org/package=SubgrpID>, R package version 0.10.
- [23] M.L. Hughes, G. Maskell, T.H. Goh, and J.L. Wilkinson, *Prospective comparison of costs and short term health outcomes of surgical versus device closure of atrial septal defect in children*, Heart 88 (2002), pp. 67–70.
- [24] J.D. Huling and M. Yu, *Subgroup identification using the personalized package*, J Stat Softw 98 (2021), pp. 1–60.
- [25] K. Imai and M. Ratkovic, *Covariate balancing propensity score*, J R Stat Soc Ser B 76 (2014), pp. 243–263.
- [26] F. Johansson, U. Shalit, and D. Sontag, *Learning representations for counterfactual inference*, in *Proc Int Conf Mach Learn*. PMLR, 2016, pp. 3020–3029.
- [27] T. Karamlou, B.S. Diggs, R.M. Ungerleider, B.W. McCrindle, and K.F. Welke, *The rush to atrial septal defect closure: is the introduction of percutaneous closure driving utilization?*, Ann Thorac Surg 86 (2008), pp. 1584–1591.
- [28] K. Lee, F. Bargagli-Stoffi, and F. Dominici, *Causal rule ensemble: interpretable inference of heterogeneous treatment effects.*, URL: <http://arxiv.org/abs/2009.09036> (2009).
- [29] C. Li, W. Li, and W. Zhu, *Penalized robust learning for optimal treatment regimes with heterogeneous individualized treatment effects*, J APPL STAT 51 (2024), pp. 1151–1170.
- [30] I. Lipkovich, A. Dmitrienko, J. Denne, and G. Enas, *Subgroup identification based on differential effect search—a recursive partitioning method for establishing response to treatment in patient subpopulations*, Stat Med 30 (2011), pp. 2601–2621.
- [31] W.J. Murdoch, C. Singh, K. Kumbier, R. Abbasi-Asl, and B. Yu, *Definitions, methods, and applications in interpretable machine learning*, Proc Natl Acad Sci 116 (2019), pp.

- 22071–22080.
- [32] E. Polley, S. Rose, and M. Laan, *Super Learning*, in *Targeted Learning: Causal Inference for Observational and Experimental Data*, chap. 3, Springer New York (2011), pp. 43–66.
 - [33] H. Qi, J. Zhao, X. Tang, X. Wang, N. Chen, W. Lv, H. Bian, S. Wang, and B. Yuan, *Open heart surgery or echocardiographic transthoracic or percutaneous closure in secundum atrial septal defect: a developing approach in one chinese hospital*, J Cardiothorac Surg 15 (2020), pp. 1–6.
 - [34] Z. Qi, Y. Liu, et al., *D-learning to estimate optimal individual treatment rules*, Electron J Stat 12 (2018), pp. 3601–3638.
 - [35] P.R. Rosenbaum and D.B. Rubin, *The central role of the propensity score in observational studies for causal effects*, Biometrika 70 (1983), pp. 41–55.
 - [36] D.B. Rubin, *Randomization analysis of experimental data: The fisher randomization test comment*, J Am Stat Assoc 75 (1980), pp. 591–593.
 - [37] H. Seibold, A. Zeileis, and T. Hothorn, *Model-based recursive partitioning for subgroup analyses*, Int J Biostat 12 (2016), pp. 45–63.
 - [38] R. Song, S. Luo, D. Zeng, H.H. Zhang, W. Lu, and Z. Li, *Semiparametric single-index model for estimating optimal individualized treatment strategy*, Electron J Stat 11 (2017), p. 364.
 - [39] X. Su, C.L. Tsai, H. Wang, D.M. Nickerson, and B. Li, *Subgroup analysis via recursive partitioning*, J Mach Learn Res 10 (2009), pp. 141–158.
 - [40] J. Tibshirani, S. Athey, E. Sverdrup, and S. Wager, *grf: Generalized Random Forests* (2022). Available at <https://CRAN.R-project.org/package=grf>, R package version 2.1.0.
 - [41] R. Tibshirani, *Regression shrinkage and selection via the lasso*, J R Stat Soc Ser B Stat Methodol 58 (1996), pp. 267–288.
 - [42] M.J. van der Laan and S. Rose, *Targeted Learning: Causal Inference for Observational and Experimental Data*, Springer, 2011.
 - [43] D. van der Linde, E.E. Konings, M.A. Slager, M. Witsenburg, W.A. Helbing, J.J. Takkenberg, and J.W. Roos-Hesselink, *Birth prevalence of congenital heart disease worldwide: A systematic review and meta-analysis*, J Am Coll Cardiol 58 (2011), pp. 2241–2247.
 - [44] B.G. Vegetabile, *On the distinction between “conditional average treatment effects”(cate) and “individual treatment effects”(ite) under ignorability assumptions*, arXiv preprint arXiv:2108.04939 (2021).
 - [45] S. Wager and S. Athey, *Estimation and inference of heterogeneous treatment effects using random forests*, J Am Stat Assoc 113 (2018), pp. 1228–1242.
 - [46] S. Wang, Y. Wang, D. Wang, Y. Yin, Y. Wang, and Y. Jin, *An improved random forest-based rule extraction method for breast cancer diagnosis*, Appl Soft Comput 86 (2020), p. 105941.
 - [47] T. Wang and C. Rudin, *Causal rule sets for identifying subgroups with enhanced treatment effects*, INFORMS J Comput 34 (2022), pp. 1626–1643.
 - [48] J. Yoon, J. Jordon, and M. van der Schaar, *GANITE: Estimation of individualized treatment effects using generative adversarial nets*, in *Int Conf Learn Represent*. 2018.
 - [49] Q.Y. Zhao, J.C. Luo, Y. Su, Y.J. Zhang, G.W. Tu, and Z. Luo, *Propensity score matching with r: Conventional methods and new features*, Ann Transl Med 9 (2021), p. 812.
 - [50] Y. Zhao, D. Zeng, A.J. Rush, and M.R. Kosorok, *Estimating individualized treatment rules using outcome weighted learning*, J Am Stat Assoc 107 (2012), pp. 1106–1118.
 - [51] X. Zhou, N. Mayer-Hamblett, U. Khan, and M.R. Kosorok, *Residual weighted learning for estimating individualized treatment rules*, J Am Stat Assoc 112 (2017), pp. 169–187.

Appendix A. The PDR framework

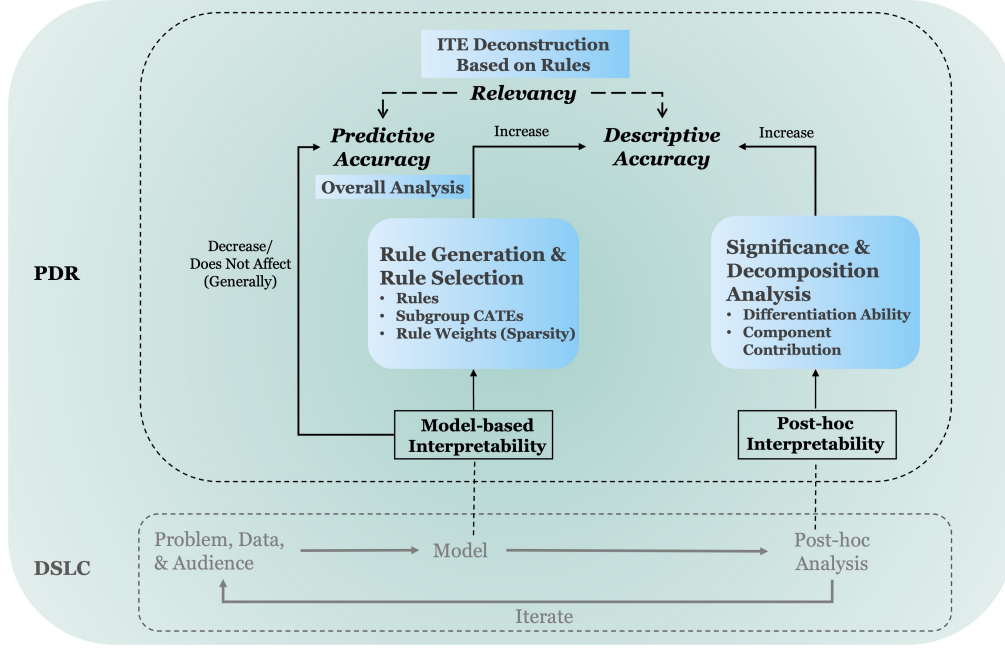


Figure A1. Overview of the PDR framework of interpretability in different stages where interpretation matters in the data-science life cycle [31]. How CRL enables PDR interpretability is also shown and highlighted in blue blocks.

The PDR framework [31] provides comprehensive guidance and a rich vocabulary for interpretability within the data science life cycle (DSLCL) in relevant research. As shown in the lower part (gray texts) of Figure A1, in a typical DSLCL, we begin with a specific domain problem for a specific audience and certain data collected to study the problem. Then, in the modeling part, we explore the data and choose certain methods to fit it. After that, we analyze what the model has learned in the post-hoc stage.

Figure A1 also presents the critical concepts in the PDR framework and their relationships in different stages of DSLCL where interpretation matters. The framework consists of three desiderata of interpretations, namely predictive accuracy, descriptive accuracy, and relevancy (italic, bold black texts in the upper part). Predictive accuracy evaluates how well the chosen model fits the data. Descriptive accuracy is the degree to which an interpretation objectively captures the relationships learned by the model. Relevancy measures how much insight an interpretation provides into the research question for a particular audience. Interpretation is also classified into model-based and post-hoc interpretability (framed bold black texts). The first interpretability involves using a simpler model to fit the data during the modeling phase to increase descriptive accuracy, in which predictive accuracy generally decreases or remains unchanged. The second one involves using various methods to extract information from a trained model to enhance descriptive accuracy. When choosing a model, there is often a trade-off between both accuracies (dashed line with a two-way arrow), i.e., whether to use a black box model with higher predictive accuracy or a simpler model with higher descriptive accuracy? The answer usually lies in relevancy determined by the problem’s specific context and its audience.

Appendix B. Three assumptions of Neyman–Rubin potential outcome framework

Below, we outline the three basic assumptions of the potential outcome framework:

1. Stable Unit Treatment Value Assumption (SUVTA): The potential outcomes of any instance do not vary with the treatments assigned to other instances and there is only one version of each treatment.

2. Ignorability/Unconfoundedness: Treatment assignment is independent of the potential outcomes conditional on the observed covariates, i.e., $A \perp \{Y(1), Y(-1)\} | X = x$. This assumption implies there are no other unmeasured confounding factors, and treatment assignment can be considered as random given the covariates X .

[35] gives an equivalent assumption conditioned on the propensity score, i.e., $A \perp \{Y(1), Y(-1)\} | \pi(a, X)$, which is especially useful in high-dimension settings where it is difficult to match samples with the original covariates. Our method is based on this assumption.

3. Positivity/Overlap: $0 < Pr(A = 1 | X = x) < 1$, i.e., any instance has a positive probability of receiving either treatment given $X = x$. This assumption ensures the existence of samples for both treatment groups so that it is possible to estimate the treatment effect.

RCT setting is usually considered to satisfy these assumptions automatically due to its deliberate design (especially the randomization on treatment assignment). However, observational data has to be pre-processed to make its treatment allocation pseudo-random to satisfy the (Conditional) Unconfoundedness Assumption and to make its sample sizes more balanced between groups to achieve an acceptable or better overlap.

Appendix C. Parameters tuning for CRL and baselines

This section outlines several parameters that require tuning when fitting CRL and other baseline models. All methods, including CRL and the baselines, are tuned using 10-fold cross-validation. The performance criteria are mean squared error (MSE) of estimators and ITE-based prediction accuracy for the simulated data and the real-world ASD data, respectively.

Table C1. Summary of parameters tuning for CRL (*min.node.size* not included).

Parameters	Tuning Range	Final value chosen
<i>num.trees</i>	{10, 50, 100, 200, 300, 400, 500, 1000, 1500, 2000}	50
<i>mtry</i>		
Simulated data	{3, 4, ..., 8, 9}	9
ASD	{4, 5, ..., 15, 16}	16
λ	100 values in [0.0004, 4] with an interval of 0.04	The one that gives the minimum mean error in 10-fold cross-validation

Table C2. Best value of *min.node.size* for CRL under different simulated data settings, tuned with 20 values in [20,400] with an interval of 20.

Number of Observations	Number of True Subgroups		
	1	3	5
2,500	70	50	80
5,000	160	80	150
10,000	300	150	190

C.1. Parameters tuning for CRL

In the rule discovery phase, we tune the parameters of CRL inherited from Causal Forest, such as *num.trees* specifying the number of trees in the forest, *min.node.size* the minimum number of samples from both treatments in each tree leaf node used to estimate the treatment effect, and *mtry* the number of variables tried for each split when fitting the forest. Other parameters of causal forest include *honesty.fraction* and *sample.fraction* specifying the sample allocation proportion in honest estimation and sample splitting, respectively. We set these two parameters to a fixed default value, i.e., 0.5. In the rule selection phase, the main parameter is λ that controls the degree of penalty in Equation (5).

For both the simulated data and the ASD data, we find that CRL’s performance is insensitive to the number of trees, so we set *num.trees* to 50 in all datasets to reduce computational costs and minimize the generation of irrelevant rules. For both the simulated data and the ASD data, we find that the performance of CRL is insensitive to the number of trees, thus we set to 50 in all data sets to save computation cost and avoid too many fake rules. *mtry* is tuned using integers from three to nine and four to sixteen, respectively, for simulated and ASD data where nine and sixteen always correspond to the lowest MSE value. For λ , the one that gives the minimum mean error is chosen from [0.0004,4]. tuning details of all the above parameters are summarized in Table C1. *min.node.size* appears to be the most sensitive parameter. Its performance is mainly affected by the number of observations and the number of pre-defined true (positive) subgroups. Details for simulated data are shown in Table C2. For ASD data, the best value is 20.

C.2. Parameters tuning for baselines

We directly use the default parameter settings for OWE and PRIM since they have few parameters that require tuning. Both CRL and CRE follow a rule-based workflow and generate rules using forest-based models. Therefore, we set CRE parameters nearly the same with CRL, namely *num.trees* to 50, and the mean depth of tree to 4. Other CRE parameters are set to default, such as learning rate to 0.01.

Similar to CRL, The best *mtry* for both CT and CF are still 9 for simulated data and 16 for the ASD data. *num.trees* of CF is 50 for all data due to its insensitivity. For *min.node.size* of CF, we find that 20 performs the best in all simulated data and 40 for the ASD data. For CT applied to the ASD data, the optimal *min.node.size* is 40 while for the simulated data, the value varies and is shown in Table C3.

Table C3. Best value of *min.node.size* for CT under different simulated data settings, tuned with 20 values in [20,400] with an interval of 20.

	Number of Observations	Number of True Subgroups		
		1	3	5
	2,500	140	180	110
	5,000	220	280	190
	10,000	50	400	280

Appendix D. Descriptive statistics of ASD variables

Table D1.: Descriptive statistics of 16 pre-treatment variables. The last two columns show the *p*-values from the two-sample *t*-test and the standardized mean difference (SMD) between the PIC and MISC groups.

Covariates	Level	PIC (positive) N=2201	MISC (negative) N=379	<i>p</i> -value	SMD
othdhis (%)	0	2154 (97.9)	373(98.4)	0.757	0.077
	1	41(1.9)	6(1.6)		
	2	5(0.2)	0(0.0)		
	3	1(0.0)	0(0.0)		
chdhis(%)	0	13(0.6)	1(0.3)	0.498	0.106
	1	1032(46.9)	195(51.5)		
	2	1147(52.1)	182(48.0)		
	3	8(0.4)	1(0.3)		
othchd (%)	4	1 (0.0)	0 (0.0)	0.002	0.221
	0	787 (35.8)	147 (38.8)		
	1	4 (0.2)	2 (0.5)		
	2	25 (1.1)	2 (0.5)		
atrial (%)	3	2 (0.1)	0 (0.0)	0.011	0.221
	4	13 (0.6)	9 (2.4)		
	5	1311 (59.6)	210 (55.4)		
	6	57 (2.6)	7 (1.8)		
NYHA (%)	7	1 (0.0)	2 (0.5)	<0.001	0.92
	8	1 (0.0)	0 (0.0)		
	0	45 (2.0)	4 (1.1)		
	1	241 (11.0)	33 (8.7)		
mesh (%)	2	1861 (84.6)	340 (89.9)	<0.001	0.33
	3	52 (2.4)	1 (0.3)		
	1	636 (29.0)	261 (68.9)		
	2	1491 (67.9)	100 (26.4)		
phth (%)	3	68 (3.1)	18 (4.7)	<0.001	0.423
	0	2071 (94.1)	318 (83.9)		
murmur (%)	1	130 (5.9)	61 (16.1)	<0.001	0.341
	0	2092 (95.0)	310 (81.8)		
	1	109 (5.0)	69 (18.2)	<0.001	0.341
	0	568 (25.8)	145 (38.3)		
	1	33 (1.5)	11 (2.9)	<0.001	0.341
	0	568 (25.8)	145 (38.3)		

continued on next page

continued from previous page.

	2	302 (13.7)	61 (16.1)		
	3	1298 (59.0)	162 (42.7)		
electb (%)	0	1401 (63.7)	108 (28.5)	<0.001	0.754
	1	800 (36.3)	271 (71.5)		
xece (%)	0	1130 (51.3)	311 (82.1)	<0.001	0.689
	1	1071 (48.7)	68 (17.9)		
sex (%)	0	985 (44.8)	148 (39.1)	0.044	0.116
	1	1216 (55.2)	231 (60.9)		
atsize0 (mean (SD))		9.41 (6.39)	17.31 (8.61)	<0.001	1.042
sysbp (mean (SD))		203.04 (13.33)	99.58 (12.07)	<0.001	0.272
diabp (mean (SD))		63.75 (10.32)	62.05 (10.68)	0.004	0.162
age (mean (SD))		10.26 (9.77)	8.74 (10.26)	0.006	0.152
BMI (mean (SD))		17.54 (5.1)	16.44 (3.60)	0.001	0.248

Table D2. Descriptive statistics of five surgery-related variables and outcome variable *HFD1Y*.

Vairables (mean (SD))	PIC (positive) N=2201	MISC (negative) N=379	p-value	SMD
<i>surgesitua</i>	1.00 (0.06)	1.01 (0.09)	0.171	0.064
<i>oroom</i>	0.22 (0.42)	0.31 (0.46)	<0.001	0.207
<i>occnum</i>	1.00 (0.13)	0.10 (0.30)	<0.001	3.858
<i>perio</i>	1.12 (0.37)	3.09 (0.82)	<0.001	3.111
<i>employ</i>	0.64 (0.48)	0.70 (0.46)	0.016	0.136
<i>HFD1Y</i>	360.05 (4.75)	352.49 (6.17)	<0.001	1.373

Generation Scenario		Variable Name	Variable Description	Variable Type
Admission	Disease History	chdhis	A cumulative value indicating whether the patient has past cardiovascular disease (CHD) and related hospital experience, like diagnoses of congenital heart disease, previous arterial dissection and previous cardiovascular surgery, etc.	Numeric (A higher value suggests a more complex and severe previous conditions of the patient)
		othdhis	A cumulative value indicating patient's history of other non-cardiovascular diseases (non-CHD) and previous hospital experience, like Trisomy 21 or other comorbidities.	
	Basic Measures	sysbp	Systolic blood pressure measured on admission	Numeric
		diabp	Diastolic blood pressure measured on admission	Numeric
		BMI	Body Mass Index (<i>weight/Height</i> ²)	Numeric
	Demographic Information	age	Age on admission	Numeric
		sex	Biological gender	Binary (1 for female and 0 for male)
Inquiry		phth	Existence of pulmonary hypertension	Binary (1 if exists and 0 otherwise)
		othchd	A cumulative value indicating whether the patient has other current conditions related to CHD, like cusp regurgitation, mitral valve stenosis, or aortic insufficiency, etc.	Numeric (A higher value suggests a more complex and severe present conditions of the patient)
Diagnosis		mesh	Indicates the current existence of comorbidities	Binary (1 if exists and 0 otherwise)
		NYHA	New York Heart Association Class, a widely-used tool to measure the degree of heart failure	Numeric (higher value indicate more severe heart conditions)
		murmur	The intensity of heart murmur.	Numeric (A value 0 indicates that there's no murmur)
Pre-surgery (treatment) Assessments and Procedures		xexe	Indicates the existence of cardiomegaly	Binary (1 if exists and 0 otherwise)
		electb	Indicates whether there exists abnormality in patient's ECG result	Binary (1 if exists and 0 otherwise)
		artial	Specifying the type of ASD	Categorical
		atsize	The size of ASD	Numeric (0 if no defect exists)
Surgery-related		periop	A cumulative value of existence of the following: Blood products usage during the perioperative period postoperative chest drainage within 24 hours and its (normalized) amount; postoperative assisted ventilation.	Numeric
		surgesitua	Timing of surgeries: elective surgeries scheduled in advance or time-limited surgeries that are required for specific timeframe.	Categorical
		oroom	Whether patient's surgery is operated at a one-stop operating room.	Binary (1 if yes and 0 otherwise)
		occnun	The number of occluders used in the surgery.	Numeric (0 if no defect exists)
		employ	Whether prophylactic antibacterial is performed.	Binary (1 for yes and 0 otherwise)

Figure D1. Description of 16 pre-treatment variables and 5 surgery-related variables.

Appendix E. Propensity score matching of the ASD data

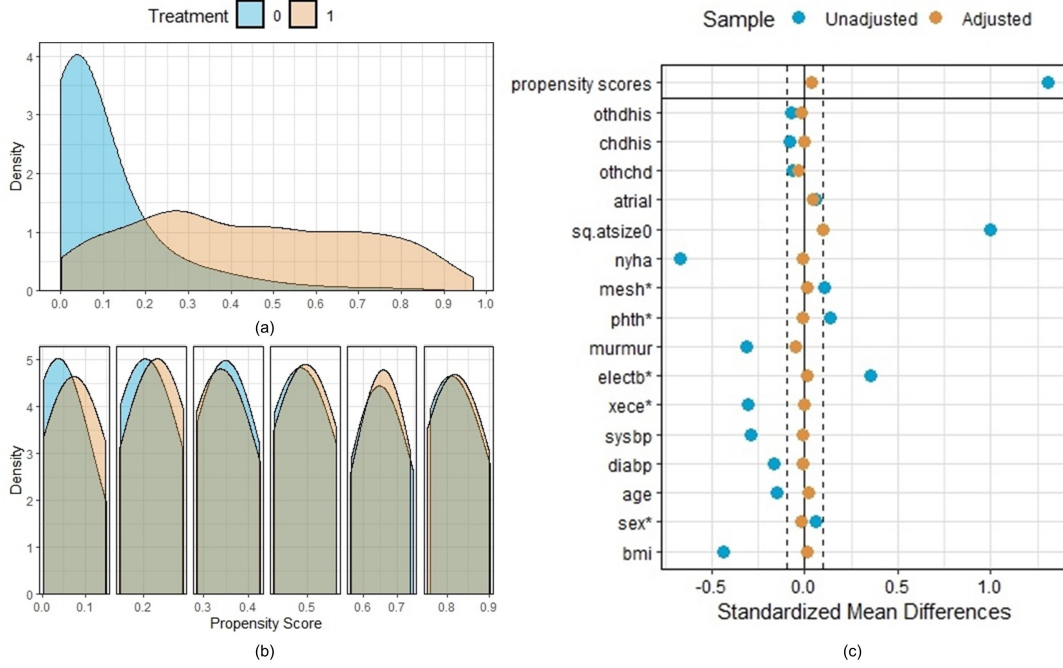


Figure E1. Details of propensity score matching on the ASD data, including the density of propensity scores before (a) and after (b) matching and love plot (c) of both treatment groups.

We use R package *MatchIt* [21] to perform the propensity score matching procedure on the pre-treatment variables of the ASD data. Note that we recode the negative treatment to 0 instead of -1 . The procedure involves three core aspects: propensity score estimation, data matching, and balance diagnostics. We measure the distance between samples in terms of propensity scores and try various combinations of propensity score estimation models and matching methods. Our final choice goes to a covariate balancing propensity score [25] model with the following implementation formula to estimate propensity scores, by which the samples are stratified into subclasses for matching:

$$treatment = othdhis + chdhis + othchd + atrial + \sqrt{atsize0} + NYHA + mesh + phth + murmur + electb + xece + sysbp + diabp + age + sex + BMI + employ.$$

This combination is able to achieve i) good overlap within each subclass, see Figure E1(b). The improvement of overlap before (Figure E1(a)) and after (Figure E1(b)) the matching is obvious; ii) balanced covariates between two treatment groups. Before the matching, there are only five variables that are considered balanced between the two groups, having a standardized mean difference (SMD) within 10%. After the matching, all covariates are balanced other than the square root of atsize0 (sq.atsize0), whose SMD value is slightly above the threshold (0.1005). Here, we consider this difference to be acceptable as it is what we can best achieve from all attempts. See the love plot in Figure E1(c) for the comparison of covariates balance between treatments before and after the matching; iii) least observations discarded. The matching process retains a total of 2554 observations, with 2180 for positive treatment (PIC) and 374 for negative treatment (MISC). We then apply CRL on this matched data set.